Revised Version

ADP-04-13/T595
JLAB-THY-04-8
DESY 04-075

ADP-04-13/T595
JLAB-THY-04-8
DESY 04-075

Precise determination of the strangeness magnetic moment of the nucleon

D. B. Leinweber, S. Boinepalli, I. C. Cloet, A. W. Thomas[†],
A. G. Williams, R. D. Young, J. M. Zanotti[*], and J. B. Zhang
Special Research Centre for the Subatomic Structure of Matter,
and Department of Physics, University of Adelaide, Adelaide SA 5005, Australia
[†] *Jefferson Laboratory, 12000 Jefferson Ave., Newport News, VA 23606 USA and*
[*] *John von Neumann-Institut für Computing NIC,*
Deutsches Elektronen-Synchrotron DESY, D-15738 Zeuthen, Germany

By combining the constraints of charge symmetry with new chiral extrapolation techniques and recent low mass lattice QCD simulations of the individual quark contributions to the magnetic moments of the nucleon octet, we obtain a precise determination of the strange magnetic moment of the proton. The result, namely $G_M^s = -0.046 \pm 0.019\ \mu_N$, is consistent with the latest experimental measurements but an order of magnitude more precise. This poses a tremendous challenge for future experiments.

arXiv:hep-lat/0406002 v2 8 Feb 2005

There is currently enormous interest in the determination of the strangeness content of the nucleon. It is crucial to our understanding of QCD to determine precisely the role played by heavier, non-valence flavors. On the experimental side new results on strangeness in the nucleon have been reported recently from JLab (HAPPEX) [1] and MIT-Bates (SAMPLE) [2]. In the near future we can expect even more precise results from the A4 experiment at Mainz as well as G0 and HAPPEX2 at JLab. By contrast, the theoretical situation is somewhat confused, with the predictions of various quark models covering an enormous range. Direct calculations within lattice QCD have not yet helped to clarify the situation, with values for G_M^s ranging from -0.28 ± 0.10 [3] to $+0.05 \pm 0.06$ [4].

We take a different approach, exploiting the advances in lattice QCD which have enabled quenched QCD (QQCD) simulations of magnetic moments at pion masses as low as 0.3–0.4 GeV [5, 6, 7, 8], as well as the development of new chiral extrapolation techniques [9, 10]. Using these techniques we determine, in full QCD, the ratios of the valence u-quark contribution to the magnetic moment of the physical proton to that in the Σ^+ and of the valence u quark in the physical neutron to that in the Ξ^0. From these ratios, the experimental values of the octet moments and charge symmetry we deduce a new theoretical value for G_M^s which is precise – setting a tremendous challenge for the next generation of parity violation experiments.

As illustrated in Fig. 1, the three point function required to extract a magnetic moment in lattice QCD involves two topologically distinct processes. (Of course, in full QCD these diagrams incorporate an arbitrary number of gluons and quark loops.) The left-hand diagram illustrates the connected insertion of the current to one of the "valence" quarks of the baryon. In the right-hand diagram the external field couples to a quark loop. The latter process, where the loop involves an s-quark, is entirely responsible for G_M^s.

Under the assumption of charge symmetry [11], the

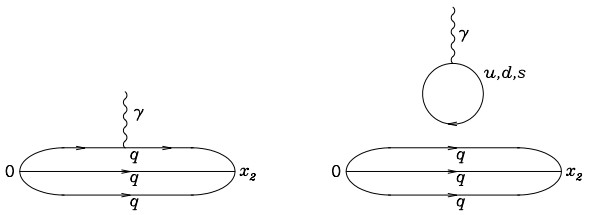

FIG. 1: Diagrams illustrating the two topologically different insertions of the current within the framework of lattice QCD.

magnetic moments of the octet baryons satisfy [12]:

$$\begin{aligned} p &= e_u\, u^p + e_d\, d^p + O_N\ ;\ n = e_d\, u^p + e_u\, d^p + O_N\,, \\ \Sigma^+ &= e_u\, u^\Sigma + e_s\, s^\Sigma + O_\Sigma\ ;\ \Sigma^- = e_d\, u^\Sigma + e_s\, s^\Sigma + O_\Sigma\,, \\ \Xi^0 &= e_s\, s^\Xi + e_u\, u^\Xi + O_\Xi\ ;\ \Xi^- = e_s\, s^\Xi + e_d\, u^\Xi + O_\Xi\,. \end{aligned} \tag{1}$$

Here, p and Ξ^- are the physical magnetic moments of the proton and Ξ^-, and similarly for the other baryons. The valence u-quark sector magnetic moment in the proton, corresponding to the LHS of Fig. 1, is denoted u^p. Charge symmetry has been used to replace the d-quark contribution in the neutron by u^p, d in the Σ^- by u in the Σ^+ (u^Σ), and so on. The labels on quark magnetic moments allow for the environment sensitivity implicit in the three-point function [12, 13]. That is, the naive expectations of the constituent quark model, namely $u^p/u^\Sigma = u^n/u^\Xi = 1$, may not be satisfied. The total contribution from quark-loops, O_N, contains sea-quark-loop contributions (RHS of Fig. 1) from u, d and s quarks. By definition

$$O_N = \frac{2}{3}\,{}^\ell G_M^u - \frac{1}{3}\,{}^\ell G_M^d - \frac{1}{3}\,{}^\ell G_M^s\,, \tag{2}$$

$$= \frac{{}^\ell G_M^s}{3}\left(\frac{1 - {}^\ell R_d^s}{{}^\ell R_d^s}\right)\,, \tag{3}$$

where the ratio of s- and d-quark *loops*, ${}^\ell R_d^s \equiv {}^\ell G_M^s / {}^\ell G_M^d$, is expected to lie in the range (0,1). Note that, in deriving Eq.(3), we have used charge symmetry

to set ${}^{\ell}G^u_M = {}^{\ell}G^d_M$. Since the chiral coefficients for the d and s loops in the RHS of Fig. 1 are identical, the main difference comes from the mass of the K compared with that of the π.

With a little algebra O_N, and hence $G^s_M (\equiv {}^{\ell}G^s_M)$, may be isolated from Eqs. (1) and (3):

$$G^s_M = \left(\frac{{}^{\ell}R^s_d}{1-{}^{\ell}R^s_d}\right)\left[2p+n-\frac{u^p}{u^\Sigma}\left(\Sigma^+-\Sigma^-\right)\right], \quad (4)$$

$$G^s_M = \left(\frac{{}^{\ell}R^s_d}{1-{}^{\ell}R^s_d}\right)\left[p+2n-\frac{u^n}{u^\Xi}\left(\Xi^0-\Xi^-\right)\right]. \quad (5)$$

Incorporating the experimentally measured baryon moments [14] (in nuclear magnetons, μ_N), Eqs. (4) and (5) become:

$$G^s_M = \left(\frac{{}^{\ell}R^s_d}{1-{}^{\ell}R^s_d}\right)\left[3.673-\frac{u^p}{u^\Sigma}\left(3.618\right)\right], \quad (6)$$

$$G^s_M = \left(\frac{{}^{\ell}R^s_d}{1-{}^{\ell}R^s_d}\right)\left[-1.033-\frac{u^n}{u^\Xi}\left(-0.599\right)\right], \quad (7)$$

We stress that *these expressions for G^s_M are exact consequences of QCD, under the assumption of charge symmetry.*

Equating (6) and (7) provides a linear relationship between u^p/u^Σ and u^n/u^Ξ which must be satisfied within QCD under the assumption of charge symmetry. Figure 2 displays this relationship by the dashed and solid line. Since this line does not pass through the point $(1.0, 1.0)$, corresponding to the simple quark model assumption of universality, there must be an environment effect exceeding 12% in both ratios or approaching 20% or more in at least one of the ratios. Indeed, a positive value for $G^s_M(0)$ would require an environment sensitivity exceeding 70% in the u^n/u^Ξ ratio!

The numerical simulations of the electromagnetic form factors presented here are carried out using the Fat Link Irrelevant Clover (FLIC) fermion action [5, 6] in which the irrelevant operators, introduced to remove fermion doublers and lattice spacing artifacts, are constructed with APE smeared links [15]. Perturbative renormalizations are small for smeared links and the mean-field improved coefficients used here are sufficient to remove $\mathcal{O}(a)$ errors from the lattice fermion action [16].

The $\mathcal{O}(a)$-improved conserved vector current [17] is used. Nonperturbative improvement is achieved via the FLIC procedure, where the terms of the Noether current having their origin in the irrelevant operators of the fermion action are constructed with mean-field improved APE smeared links. The results presented here are obtained using established techniques [18] from a sample of 400 $20^3 \times 40$ mean-field $\mathcal{O}(a^2)$-improved Luscher-Weisz [19] gauge field configurations having a lattice spacing of 0.128 fm, determined by the Sommer scale $r_0 = 0.50$ fm.

One of the major challenges in connecting lattice calculations of hadronic properties with the physical world

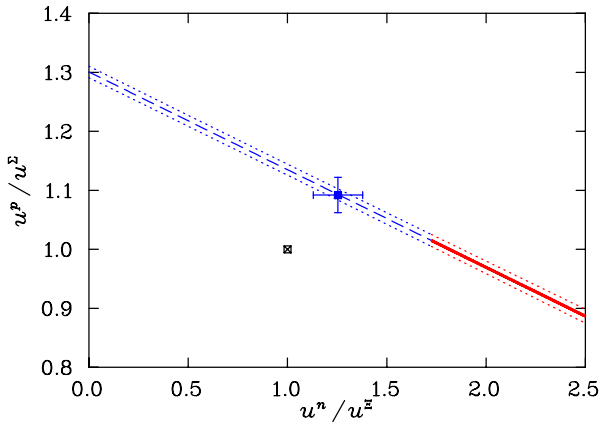

FIG. 2: The constraint (dashed $G^s_M(0) < 0$, solid $G^s_M(0) > 0$) on the ratios u^p/u^Σ and u^n/u^Ξ implied by charge symmetry and experimental moments. Experimental uncertainties are indicated by the dotted bounds. The assumption of environment independent quark moments is indicated by the crossed square. Our final result (chiral corrected extrapolation of lattice results) is illustrated by the filled square on the charge symmetry line.

[20] is that currently accessible quark masses are much larger than the physical values. Our present analysis has been made possible by a significant breakthrough in the regularization of the chiral loop contributions to hadron observables [9, 10, 21]. Through the process of regulating loop integrals via a finite-range regulator [9, 22], the chiral expansion is effectively re-summed to produce an expansion with vastly improved convergence properties. In particular, we extrapolate FLIC fermion calculations of the valence quark contributions to baryon moments (u^p, u^n, u^Σ, u^Ξ) to the physical mass regime. We select the dipole-vertex FRR with $\Lambda = 0.8$ GeV, which yields the best simultaneous description of both quenched and dynamical simulation results [23].

Separation of the valence and sea-quark-loop contributions to the meson cloud of full QCD hadrons is a non-trivial task. We use the diagrammatic method for evaluating the quenched chiral coefficients of leading non-analytic terms in heavy-baryon quenched χPT (QχPT) [24, 25]. The valence contributions (key to this analysis) are obtained by removing the direct-current coupling to sea-quark loops from the total contributions. Upon further removing "indirect sea-quark loop" contributions, where a valence quark forms a meson composed with a

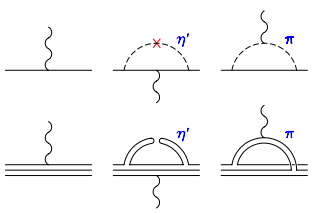

FIG. 3: Diagrams providing the leading contributions to the chiral expansion of baryon magnetic moments (upper diagrams) and their associated quark flows (lower diagrams) in QQCD.

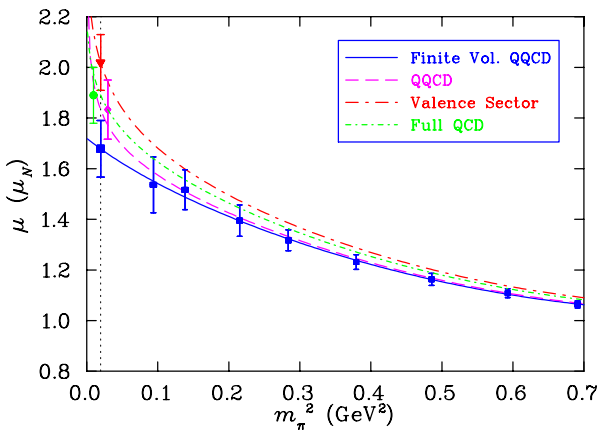

FIG. 4: The contribution of a single u quark (with unit charge) to the magnetic moment of the proton. Lattice simulation results (square symbols for $m_\pi^2 > 0.05$ GeV) are extrapolated to the physical point (vertical dashed line) in finite-volume QQCD as well as infinite volume QQCD, valence and full QCD – see text for details. Extrapolated values at the physical pion mass (vertical dashed line), are offset for clarity.

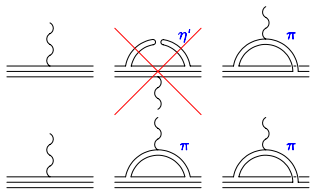

FIG. 5: Correcting QχPT (upper) to the valence sector of full QCD (lower diagrams). We remove quenched negative-metric η' contributions and adjust the chiral coefficients of π and K loops to account for the coupling of a valence quark to the photon in a meson made from a sea-quark loop. Coupling to the anti-quark in the bottom-right diagram is also included in the valence contribution of full QCD.

sea-quark loop, one obtains the "quenched valence" contributions – the conventional view of the quenched approximation.

Figure 3 displays the diagrams providing the leading contributions to the chiral expansion of baryon magnetic moments (upper diagrams) and their associated quark flows in quenched QCD (QQCD). The associated chiral expansion for the proton magnetic moment, μ_p, has the form

$$\begin{aligned}\mu_p &= a_0^\Lambda + \mu_p\,\chi_{\eta'}\,I_{\eta'}(m_\pi,\Lambda) + \chi_{\pi B}\,I_B(m_\pi,\Lambda) \\ &\quad + \chi_{KB}\,I_B(m_K,\Lambda) + a_2^\Lambda\,m_\pi^2 + a_4^\Lambda\,m_\pi^4\,. \qquad (8)\end{aligned}$$

where the repeated index, B, sums over allowed baryon octet and decuplet intermediate states. Loop integrals denoted by I are defined by

$$I_B(m,\Lambda) = -\frac{2}{3\pi}\int dk\,\frac{\left(2\sqrt{k^2+m^2}+\Delta_{BN}\right)\,k^4\,u^2(k,\Lambda)}{(k^2+m^2)^{3/2}\,\left(\sqrt{k^2+m^2}+\Delta_{BN}\right)^2}\,, \qquad (9)$$

$$I_{\eta'}(m_\pi,\Lambda) = -\int_0^\infty dk\,\frac{k^4}{(k^2+m_\pi^2)^{\frac{5}{2}}}u^2(k,\Lambda)\,, \qquad (10)$$

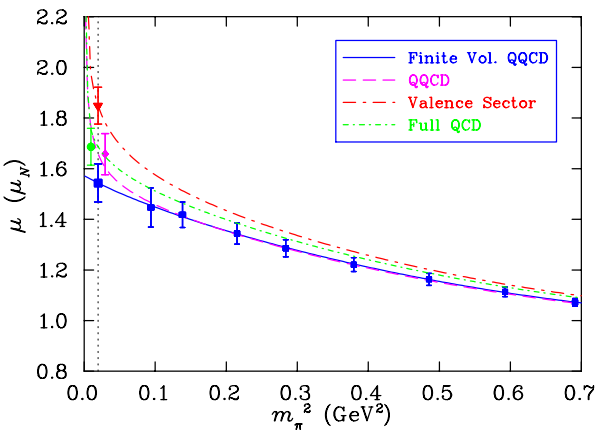

FIG. 6: The contribution of a single u quark (with unit charge) to the magnetic moment of the Σ^+. Curves and symbols are as for Fig. 4.

where Δ_{BN} is the relevant baryon mass-splitting and $u(k,\Lambda)$ is the dipole-vertex regulator. The coefficients, χ, denote the known model-independent coefficients of the LNA term for π and K mesons [25, 26]. We take $m_K^2 = m_K^{(0)\,2} + \frac{1}{2}\,m_\pi^2$, and use the physical values to define $m_K^{(0)}$. The m_π^4 term in Eq. (8) allows for some curvature associated with the Dirac moment of the baryon, which should go as $1/m_\pi^2$ for moderately large quark masses.

Figure 4 illustrates a fit of FRR QχPT to the FLIC fermion lattice results (solid curve), where only the discrete momenta allowed in the finite volume of the lattice are summed in performing the loop integral. The long-dashed curve that also runs through the lattice results corresponds to replacing the discrete momentum sum by the infinite-volume, continuous momentum integral. For all but the lightest quark mass, finite volume effects are negligible.

The coefficients of the residual expansion, a_0^Λ, a_2^Λ, a_4^Λ, show excellent signs of convergence. For example, the fit to u^Σ yields values 1.48(7), −0.90(23), and 0.42(19) in appropriate powers of GeV, respectively. Incorporating baryon mass splittings into the kaon loop contributions is essential – e.g., the contribution of $\Sigma \to NK$ is almost doubled when the $\Sigma - N$ mass splitting is included.

Figure 5 illustrates the considerations in correcting the quenched u-quark contribution to yield the valence u-quark contribution in full QCD. The removal of quenched η' contributions and the appropriate adjustment of π and K loop coefficients [24, 25, 26] provides the dot-dash curve of Fig. 4. This is our best estimate of the valence u-quark contribution (connected insertion) to the proton magnetic moment of full QCD. Finally, the disconnected insertion of the current is included to estimate the total contribution of the u-quark sector to the proton magnetic moment [24, 25, 26] (fine dash-dot curve in Fig. 4). Figure 6 displays similar results for the Σ^+.

From these chiral extrapolations, we estimate the ratios of the valence (connected) u-quark contributions,

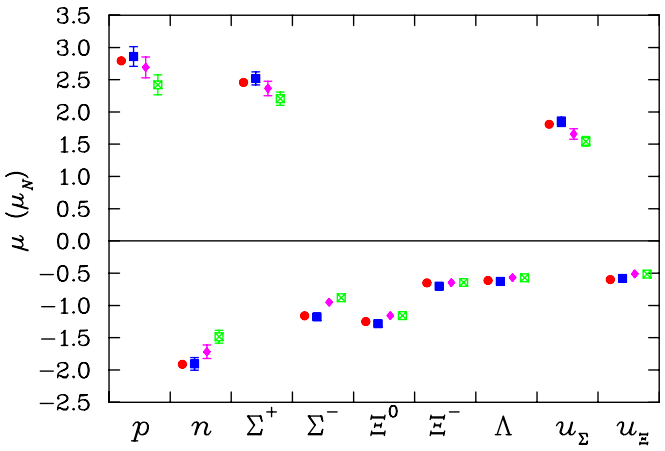

FIG. 7: The one standard deviation agreement between the FRRχPT corrected lattice simulation results (■) and the experimentally measured baryon magnetic moments (•). Quenched (⧫) and finite-volume quenched (⊠) results are also illustrated.

u^p/u^Σ and u^n/u^Ξ. The final results

$$\frac{u^p}{u^\Sigma} = 1.092 \pm 0.030 \quad \text{and} \quad \frac{u^n}{u^\Xi} = 1.254 \pm 0.124 \qquad (11)$$

are plotted in Fig. 2. The precision of these results follows from the use of correlated ratios of moments which act to reduce uncertainties associated with the lattice spacing, the regulator mass and statistical fluctuations [27]. This result leaves no doubt that G_M^s is negative. The fact that this point lies exactly on the constraint curve is highly nontrivial, and provides a robust check of the validity of the analysis techniques presented here.

As a further check, in Fig. 7 we compare the lattice QCD predictions of the baryon magnetic moments constructed from chirally-corrected extrapolations of the individual quark sectors. The results display an unprecedented level of agreement with experiment. We note that the experimental constraints on u^Σ and u^Ξ emphasized by Wong [28] are both satisfied precisely.

While G_M^s is most certainly negative, it remains to set the magnitude. This requires an estimate of the strange to light sea-quark loop contributions, ${}^\ell R_d^s$. Earlier estimates of ${}^\ell R_d^s$ were based on the constituent quark model. A more reliable approach is to estimate the loops using the same successful model invoked to correct the quenched results to full QCD [10, 23] as illustrated in Fig. 7. Allowing the dipole mass parameter to vary between 0.6 and 1.0 GeV provides ${}^\ell R_d^s = G_M^s/G_M^d = 0.139 \pm 0.042$. A complete analysis of the errors associated with the determination of G_M^s using Eqs. (4), (5) and (11) is reported in Ref. [27]. The uncertainty is dominated by the statistical errors included in Eq. (11) and the uncertainty just noted for ${}^\ell R_d^s$. The final result for the strangeness magnetic moment of the nucleon is

$$G_M^s = -0.046 \pm 0.019 \ \mu_N \, . \qquad (12)$$

This precise value sets a tremendous challenge for the next generation of parity violation experiments.

We thank the Australian Partnership for Advanced Computing (APAC) for generous grants of supercomputer time which have enabled this project. This work is supported by the Australian Research Council and by DOE contract DE-AC05-84ER40150, under which SURA operates Jefferson Laboratory.

[1] K. A. Aniol *et al.* [HAPPEX Collaboration], Phys. Lett. B **509**, 211 (2001) [nucl-ex/0006002].
[2] D. T. Spayde *et al.* [SAMPLE Collaboration], Phys. Lett. B **583**, 79 (2004) [arXiv:nucl-ex/0312016].
[3] N. Mathur and S. J. Dong, Nucl. Phys. Proc. Suppl. **94**, 311 (2001) [hep-lat/0011015]; S. J. Dong, *et al.*, Phys. Rev. **D58**, 074504 (1998) [hep-ph/9712483].
[4] R. Lewis, W. Wilcox and R. M. Woloshyn, Phys. Rev. D **67**, 013003 (2003) [hep-ph/0210064].
[5] J. M. Zanotti *et al.* [CSSM Lattice Collaboration], Phys. Rev. D **65**, 074507 (2002) [hep-lat/0110216].
[6] D. B. Leinweber *et al.*, Eur. Phys. J. A **18**, 247 (2003) [nucl-th/0211014].
[7] J. M. Zanotti, B. Lasscock, D. B. Leinweber, and A. G. Williams, hep-lat/0405015.
[8] J. M. Zanotti, S. Boinepalli, W. Kamleh, D. B. Leinweber, and A. G. Williams, hep-lat/0405026.
[9] R. D. Young, D. B. Leinweber and A. W. Thomas, Prog. Part. Nucl. Phys. **50**, 399 (2003) [hep-lat/0212031].
[10] R. D. Young, D. B. Leinweber and A. W. Thomas, Phys. Rev. D **71**, 014001 (2005) [arXiv:hep-lat/0406001].
[11] G.A. Miller *et al.*, Phys. Rept. **194**, 1 (1990).
[12] D.B. Leinweber, Phys. Rev. **D53**, 5115 (1996) [hep-ph/9512319].
[13] D. B. Leinweber and A. W. Thomas, Phys. Rev. D **62**, 074505 (2000) [hep-lat/9912052].
[14] Particle Data Group, Phys. Rev. **D66**, 010001 (2002).
[15] M. Falcioni *et al.*, Nucl. Phys. **B251**, 624 (1985).
[16] S. O. Bilson-Thompson *et al.*, Ann. Phys. **304**, 1 (2003) [hep-lat/0203008].
[17] G. Martinelli *et al.*, Nucl. Phys. B **358**, 212 (1991)
[18] D. B. Leinweber *et al.*, Phys. Rev. **D43**, 1659 (1991).
[19] M. Luscher and P. Weisz, Commun. Math. Phys. **97**, 59 (1985) [ibid. **98**, 433 (1985)].
[20] T. D. Cohen and D. B. Leinweber, Comments Nucl. Part. Phys. **21**, 137 (1993) [hep-ph/9212225]; A.W. Thomas, Austral. J. Phys. **44**, 173 (1991).
[21] D. B. Leinweber, A. W. Thomas and R. D. Young, Phys. Rev. Lett. **92**, 242002 (2004) [hep-lat/0302020].
[22] J. F. Donoghue, *et al.*, Phys. Rev. **D59**, 036002 (1999).
[23] R. D. Young *et al.*, Phys. Rev. D **66**, 094507 (2002) [hep-lat/0205017].
[24] D. B. Leinweber, Nucl. Phys. Proc. Suppl. **109A**, 45 (2002) [hep-lat/0112021].
[25] D. B. Leinweber, Phys. Rev. D **69**, 014005 (2004) [hep-lat/0211017].
[26] M. J. Savage, Nucl. Phys. A **700**, 359 (2002) [nucl-th/0107038].
[27] D. B. Leinweber, *et al.*, hep-lat/0502004.
[28] C. W. Wong, hep-lat/0103021.